Carbohydrate Polymers 121 (2015) 217–223

Contents lists available at ScienceDirect

Carbohydrate Polymers

journal homepage: www.elsevier.com/locate/carbpol

Maltodextrin fast dissolving films for quercetin nanocrystal delivery. A feasibility study

Francesco Lai[a], Ilaria Franceschini[b], Francesco Corrias[a], Maria Chiara Sala[b], Francesco Cilurzo[b], Chiara Sinico[a,*], Elena Pini[b]

[a] Dept. Scienze della Vita e dell'Ambiente, University of Cagliari, Cagliari 09124, Italy
[b] Dept. Scienze Farmaceutiche, University of Milan, Milan 20133, Italy

ARTICLE INFO

Article history:
Received 29 July 2014
Received in revised form
27 November 2014
Accepted 29 November 2014
Available online 31 December 2014

Keywords:
Maltodextrins
Quercetin
Nanocrystals
Fast dissolving films

ABSTRACT

The objective of this study was to evaluate the feasibility to prepare fast dissolving films as quercetin nanocrystal delivery systems, using maltodextrins as film forming material and glycerin as plasticizer, with the goal of enhancing quercetin oral bioavailability. Quercetin nanosuspensions were prepared using a high-pressure homogenizer, and then directly used to prepare the films by a casting method. Spectroscopic and calorimetric analysis evidenced that reduction of quercetin size at nanoscale and incorporation in maltodextrin films do not affect the solid state of the active ingredient. The loading of quercetin nanocrystals into the film determined a slight variation of film elasticity and ductility. Indeed, the elastic modulus of the loaded films resulted about a half of the placebo ones, while the elongation at break increased four folds. Free and film loaded quercetin nanocrystals showed a comparable dissolution rate, much higher than that of bulk quercetin.

© 2015 Elsevier Ltd. All rights reserved.

1. Introduction

Quercetin (3,3,4,5,7-pentahydroxyflavone, QUE), one of the most common dietary polyphenols widely found in the plant kingdom including vegetables, fruits, medicine herbs and red wine, has been intensively investigated for its anti-inflammatory, antioxidant, antiviral, anticarcinogenic and cardioprotective properties (Nijveldt et al., 2001), without any evidence of toxicity, carcinogenicity or genotoxicity related to consumption (Harwood et al., 2007; Okamoto, 2005; Utesch et al., 2008). In the western world, the average daily intake of QUE has been estimated to be between 20 mg and 40 mg, but more research is necessary to establish the dosage required to achieve health effects while avoiding toxicity (Kelly, 2011). Moreover, biomedical applications of this natural compound are severally hampered by its low oral bioavailability due to poor water solubility and rapid metabolism (Cai, Fang, Dou, Yu, & Zhai, 2013).

To overcome these issues, several formulation approaches have been developed, involving the use of drug delivery systems such as cyclodextrin inclusion complexes, liposomes, micelles, and nanoparticles, which provide higher water solubility and bioavailability (Chessa et al., 2011; Fatma et al., 2014; Ribeiro et al., 2009; Zheng & Chow, 2009). Moreover, it has been reported that systems based on solid dispersions of quercetin in polymer matrices, are a promising approach for developing quercetin formulations with enhanced oral bioavailability. Polymer matrices include polyethylene glycol (Li, Zhang, Deng, & Liang, 2004), polyvinylpirrolidone (De Mello Costa et al., 2010) and, recently, cellulose derivative (Li et al., 2013).

Among the several strategies widely described in the literature, drug nanocrystal technologies are considered one of the most valuable approaches to formulation of poorly soluble drugs (Kocbek, Baumgartner, & Kristl, 2006; Müller, Gohla, & Keck, 2011). These technologies produce dispersions of drug nanocrystals in a liquid medium (typically water), which has to be eliminated by means of specialized techniques (spray drying or freeze drying) to obtain the final solid dosage form, namely tablets, capsules, granules and pellets. The main challenge in developing solid nanoparticle formulations is the redispersibility of dried drug nanoparticles that must have the ability to return to their original size (Lai et al., 2011; Van Eerdenbrugh et al., 2008). Interestingly, drug nanocrystals have been recently proposed in combination with the novel fast dissolving film technology (Shen et al., 2013). In this case, the nanosuspension was mixed with an aqueous solution containing fast dissolving film components and the final blend was casted and dried, thus obtaining a nanocrystal-loaded film, which was cut to

* Corresponding author. Tel.: +39 070 6758555.
E-mail address: sinico@unica.it (C. Sinico).

http://dx.doi.org/10.1016/j.carbpol.2014.11.070
0144-8617/© 2015 Elsevier Ltd. All rights reserved.

the desired size. However, also in this case one of the main issues associated with the production of these dosage forms is nanocrystal aggregation and growth. Indeed, fast dissolving films can be made of polysaccharide polymers plasticized by low molecular weight excipients, such as glycerin, polyethylene glycol or propylene glycol, which could cause a physical instability of the drug nanocrystals.

The first polysaccharide employed to produce fast dissolving films was pullulan, a glucan consisting of maltotriose units obtained by the fungus *Aureobasidium pullulans* (Leathers, 2003). Pullulan can be considered the most suitable excipient for the design of these dosage forms since it presents favorable rheological and mechanical properties and processability. Nevertheless, its use is limited by the low availability and high costs. Thus, other edible hydrocolloids such as modified starches and cellulose ethers have been proposed as substitutes (Pinna & Pinna, 2009; Zerbe & Guo, 1998). The possibility of using maltodextrin (MDX) as film forming material and glycerin as plasticizer has been also demonstrated (Cilurzo et al., 2010; Selmin, Franceschini, Cupone, Minghetti, & Cilurzo, 2015).

MDX are water-soluble biopolymers obtained from the partial hydrolysis of food grade starch. They contain linear amylase, branched amylopectin and a relatively small amount of dextrose and maltose. D-Glucose units are primarily linked by α-(1,4) bonds, but there are also branched segments linked by α-(1,6) bonds. MDXs, which can differ in average molecular size, are commonly classified by their dextrose equivalent (DE) values, defined as the percentage of reducing sugars calculated as glucose on a dry substance basis. Several physical and functional characteristics are influenced by the DE such as solubility, freezing temperature and viscosity (Garnero, Chattah, & Longhi, 2013).

The purpose of this study was to evaluate the feasibility of preparation of orodispersible fast dissolving films containing QUE nanocrystals, using maltodextrins as film forming material and glycerin as plasticizer (Cilurzo et al., 2010; Cilurzo, Cupone, Minghetti, Selmin, & Montanari, 2008), with the purpose of enhancing QUE oral bioavailability bioavailability. Indeed, these films, when placed onto or under the tongue disintegrate in a short time favoring the local drug absorption, avoiding first-pass hepatic metabolism. Moreover, they are useful for patients who have difficulty in swallowing (Shen et al., 2013).

In this work, QUE nanosuspensions were prepared using a high pressure homogenizer (Lai et al., 2014), and then directly used for drying by lyophilisation or preparing the fast dissolving films. The solid state of bulk QUE, QUE nanocrystals and QUE films were investigated by means of FTIR, DSC and XRPD analyses. Moreover, QUE nanocrystals were characterized by photon correlation spectroscopy for mean size and size distribution and by transmission electron microscopy for morphological studies. The dissolution profile of QUE nanocrystal-loaded films was compared to that of freeze dried QUE nanocrystals and bulk QUE. Furthermore, the effect of nanocrystals on fast dissolving film tensile properties was investigated.

2. Materials and methods

2.1. Materials

Maltodextrin having a D.E. equal to 6 and molecular mass 2720 g/mol (Glucidex® IT6, MDX6) was obtained by Roquette, (France). Glycerin (GLY) and sorbitan monooleate (Span® 80, S80) were purchased from Carlo Erba Reagenti (Italy) and Croda (Italy), respectively. Polysorbate 80 (Tween® 80, T80) was purchased from Galeno (Italy) and QUE was purchased from Sigma-Aldrich (Italy). All solvents were of analytical grade, unless otherwise specified.

2.2. QUE nanosuspension preparation

QUE nanosuspensions were prepared by high pressure homogenization. 5% (w/w) QUE coarse powder was dispersed in water with 1% (w/w) Tween 80 and disintegrated into microsuspensions by a high shear homogenizer (Ultra-Turrax® T25, IKA, Germany) at 12.000 rpm for 5 min. Obtained microsuspensions were homogenized at high pressure using a high pressure homogenizer (EmulsiFlex-C5, Avestin Inc., Ottawa, Canada). At first, 5 cycles at 500 bar were conducted as pre-milling step, and then 20 cycles at 1000 bar were run to obtain the nanosuspension. The obtained nanosuspensions were freeze dried or directly used to obtain fast dissolving films containing QUE nanocrystals.

2.3. Fast dissolving film preparation

Films were prepared modifying the solvent casting technique previously described (Cilurzo et al., 2008). Briefly, drug loaded films were obtained by gradually adding MDX6 to a QUE nanosuspension under magnetic stirring until the film forming material was completely dissolved. Afterwards, GLY and S80 were added. The component amounts were set in order to have a MDX6/GLY/S80 ratio of 76/21/3 w/w (film thickness was set to achieve a final weight of about 100 mg/6 cm^2) and a final drug content of 10 mg/6 cm^2. To better investigate the QUE solid state, a placebo formulation with the same composition, including the Tween 80 used for the production of the nanosuspension but without quercetin was also prepared as control.

After a rest period of 16 h, slurries were cast over a silicone release liner by a laboratory-coating unit Mathis LTE-S(M) (Switzerland). Operative conditions: coating rate: 1 m/min; drying temperature: 50 °C; drying time: 20 min; air circulation speed: 1200 rpm. Films were cut into suitable shape and size as required for testing, packed immediately after the preparation in individual airtight aluminum seal packs and stored at 25 °C until use. Placebo films were also prepared following the same procedure.

2.4. Analytical characterization

Infrared absorption spectra were recorded on a Perkin Elmer (MA, USA) FTIR Spectrometer "Spectrum One" in the middle infrared region (4000 and 450 cm^{-1}). The solid samples, mixed in a mortar with KBr (1:100), were pressed in a hydraulic press (9 tons) to small tablets and analyzed by transmittance technique with 8 signal-averaged scans collected at a spectral resolution of 4 cm^{-1}.

The XRPD analyses were carried out by using a Rigaku Miniflex diffractometer. The setting parameters were Ni-filtered Cu*K*α radiation detector (λ = 1.5405 Å), voltage of 30 kV, current of 15 mA, scan angular speed 2°/min and scan step time 2.00 s in the 2θ range from 3° to 60°. The XRPD patterns of QUE raw material, freeze dried QUE nanocrystal, QUE nanocrystal-loaded films and placebo films were recorded. The films were cut in disks of a diameter comparable with that of the aluminum sample plate and then analyzed in the conditions above described.

The DSC curves of the different samples were recorded on a Perkin Elmer DSC 6 differential scanning calorimeter calibrated with indium. The thermal behavior was studied by heating 2.5 mg samples in aluminum crimped pans under nitrogen gas flow. The samples were heated from 25 °C to 100 °C at 10 °C/min to eliminate moisture, quickly cooled at 25 °C and then heated from 25 °C to 350 °C at 10 °C/min; reported thermograms refer to the second heating scan.

2.5. Particle size and zeta potential measurements

QUE nanosuspensions were analyzed for particle size and zeta potential by photon correlation spectroscopy (PCS) using a Zetasizer Nano ZS (Malvern Instruments, UK). Samples were backscattered by a helium–neon laser (633 nm) at an angle of 173° and a constant temperature of 25 °C. The instrument systematically and automatically adapts to the sample by adjusting the intensity of the laser and the attenuator of the photomultiplier, thus ensuring reproducibility of the experimental measurement conditions. Zeta potential was estimated using the Zetasizer nano-ZS by means of the M3-PALS (Phase Analysis Light Scattering) technique. All the samples were analyzed 24 h after preparation. A long-term stability study of formulations stored at 4 ± 1 °C was performed by monitoring formulation average size, polydispersity and surface charge over 90 days. Particle size and zeta potential of film loaded with QUE nanocrystals were measured after dispersion of films in Milli®Q water. The presence of possible coarse aggregates was investigated by using an Accusizer 770 granulometer (P SS Inc., Santa Barbara, USA). The results are expressed as the mean of three determinations.

2.6. Film thickness

Film thickness was measured by using a MI 1000 Micrometer (ChemInstruments, USA, range of measurement 0–50 mils (0–1270 μm, accurate to ±0.2% of range). Before sample cutting, film was placed between the anvil and the presser foot of the micrometer.

2.7. Tensile properties

Tensile testing was conducted using a tensile testing machine equipped with a 50 N load cell (Instron 5965, ITW Test and Measurement Italia S.r.l., Trezzano sul Naviglio, Italy).

The film was cut into 80 × 15 mm strips and equilibrated at 25 °C. Tensile tests were performed according to the procedure reported in a previous work (Cilurzo et al., 2010). Each test strip was longitudinally placed in the tensile grips on the texture analyzer. Initial grip separation was 40 mm and crosshead speed was 25 mm/min.

The test was considered concluded at the film break. Tensile strength, elongation at break, elastic modulus and work were computed to evaluate the tensile properties of the films.

Tensile strength (TS) was calculated by dividing the maximum load by the original cross-sectional area of the specimen and it was expressed in force per unit area (MPa).

Percent elongation at break (*E*%) was calculated by dividing the extension at the moment of specimen rupture by the initial specimen gage length and multiplying by 100 according to the following equation:

$$E\% = \frac{L - L_0}{L_0} \times 100 \quad (1)$$

where L_0 is the initial gage length of the specimen and L is the length at the moment of rupture.

Elastic modulus or *Young's modulus* (*Y*) was calculated as the slope of the linear portion of the stress–strain curve. The result was expressed in force per unit area (MPa).

Tensile energy to break (*W*) was defined by the area under the stress–strain curve. The value is in units of energy.

An average of five measurements was taken for each type of specimen.

2.8. Transmission electron microscopy (TEM)

Morphology of freeze dried QUE nanocrystals, placebo film and QUE nanocrystal-loaded film was visualized by using transmission electron microscopy (Tecnai 12, FEI, operating at 120 kV). To analyze nanosuspensions a drop of preparation and an equal volume of an aqueous 1% uranyl acetate solution were adsorbed on the surface of a copper grid and dried at room temperature for 24 h. Placebo and drug loaded film, instead, were put in an aluminum stub without any reagent and then analyzed.

2.9. In vitro dissolution studies

In vitro dissolution studies of QUE raw material, freeze dried QUE nanocrystals and QUE nanocrystal-loaded films were performed according to the United States Pharmacopeia (USP) using the rotating basket method (Erweka apparatus). The dissolution medium was 1000 ml of distilled water kept at 37 ± 0.1 °C and stirred at a rotation speed of 100 ± 2 rpm. At preselected time intervals, a 1 ml sample was withdrawn (replaced with 1 ml of pre-thermostated fresh dissolution medium), filtered through a polycarbonate membrane (0.45 μm, Millipore) and analyzed by HPLC at 367 nm, using a chromatograph Alliance 2690 (Waters, Milan, Italy). The column was a SunFire C18 (3.5 m, 4.6 × 150 mm). The mobile phase was a mixture of acetonitrile, water and acetic acid (94.8:5.0:0.2 v/v), delivered at a flow rate of 1.0 ml min^{-1}. Dissolution tests were performed in triplicate.

At each sampling time, percentage data were arc-sin transformed and then analyzed using one-way ANOVA, with three treatment formulations and three replicates, and LSD procedure for pair comparison among means.

3. Results and discussion

3.1. Solid state characterization

In order to elucidate the effects of formulation processes on drug crystalline properties, the solid state of bulk QUE, freeze dried QUE nanocrystals, QUE nanocrystal-loaded film was investigated using XRPD, FTIR and DSC techniques. To better investigate these multicomponent formulations a placebo film without QUE nanocrystals was prepared and used as reference in the analytical study. As previously reported in the literature (Sahoo et al., 2011), QUE XRPD analysis showed a semi-crystalline pattern with typical reflection peaks at 4.54°, 9.78°, 13.06°, 26.00°, 27.92° 2θ.The freeze-dried nanocrystal diffractograms showed some diffraction peaks ascribable to crystalline QUE at a diffraction angle of 2θ 4.48°, 12.42°, 27.42° (Fig. 1) although a few peaks were shifted. The differences in peak relative intensities and the partial amorphisation are probably due to the high pressure homogenization process. Indeed, as previously demonstrated, during homogenization, cavitation forces as well as collision and shear forces determine break down of the drug particles down to the nanometer range. These high energy forces can also induce a change in crystal structure and/or partial or total amorphisation of the sample.

As depicted in Fig. 1, the placebo film diffractogram showed a typical amorphous pattern, without any crystalline domain, while the QUE nanocrystal-loaded film diffractogram exhibited a residual crystallinity attributable to QUE.

In Fig. 2, the thermal behavior of QUE, QUE nanocrystals, film loading QUE, film loading nanocrystals and placebo film are reported. The QUE raw material DSC analysis presented a sharp endothermic peak at 318 °C (onset temperature) while the freeze dried nanocrystal thermal behavior showed a melting peak at an onset temperature of 293 °C, slightly shifted to lower temperature

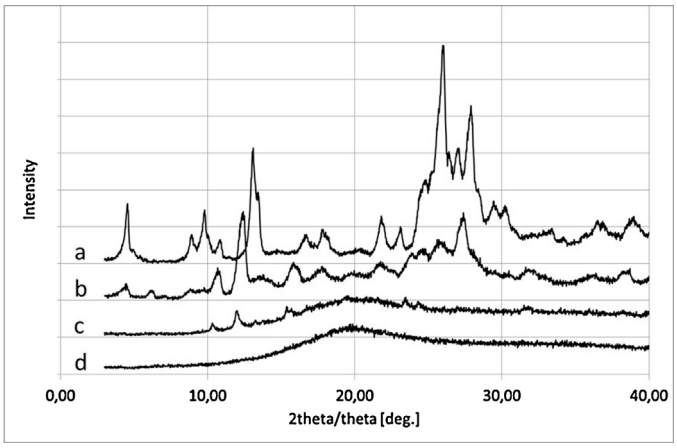

Fig. 1. Diffraction patterns of bulk QUE (a), QUE nanocrystals (b), film loading QUE nanosuspension (c) and placebo film (d).

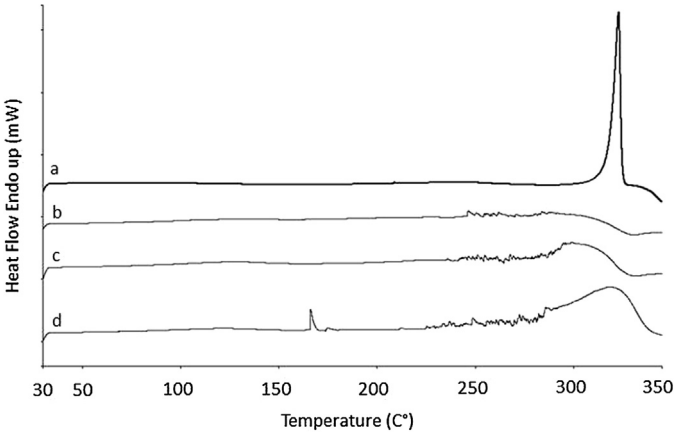

Fig. 2. Thermograms of bulk QUE (a), QUE nanocrystals (b), film loading QUE nanosuspension (c), film loading QUE(d) and placebo film (e).

due to loss of crystallinity and/or for the presence of the formulation excipients. The ΔH_f decrease from 163.68 J/g (QUE) up to 63.90 J/g (QUE nanocrystals) confirmed the loss in crystallinity due to high pressure homogenization (Sahoo et al., 2011). In both the QUE-loaded and the nanocrystalline QUE-loaded films, no endothermic peak attributable to QUE melting was detectable, possibly due to masking by thermal degradation of the film components when sorbitan monooleate is used as surfactant (Cilurzo et al., 2008).

Bulk QUE FTIR spectrum evidenced in the region between 3400 and 3000 cm^{-1} the strong O—H deformation band partially overlapped to the Csp^2—H stretching; at 1672, 1615 and 1513 cm^{-1} the C=O and C=C stretchings, respectively.

The FTIR spectrum of lyophilized QUE nanocrystals is almost superimposable upon that of QUE, but absorption bands at 2920, 2852 and 1729 cm^{-1} attributable to C—H and C=O Tween 80 stretchings are also visible. The placebo film and the QUE nanocrystal-loaded films were also analyzed; both spectra showed strong broad bands imputable to MDX; however, the characteristics peaks of nanosuspension (QUE C=O and C=C stretchings) in the range between 1740 and 1520 cm^{-1} are still visible in the QUE nanocrystal-loaded film spectrum (Fig. 3).

In conclusion, XRPD data evidenced that the reduction of QUE size at nanoscale do not alter the QUE solid state and moreover, the incorporation in the MDX fast dissolving films do not transform the active ingredient into a completely amorphous state.

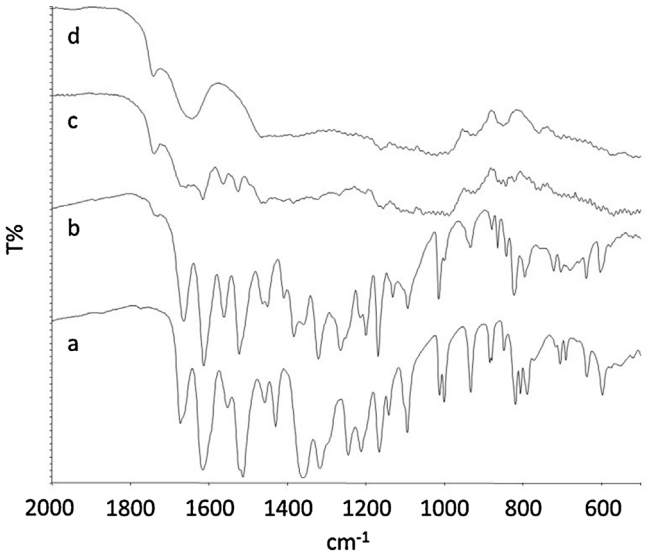

Fig. 3. FTIR spectra in the 2000–600 cm^{-1} range: bulk QUE (a), QUE nanocrystals (b), film loading QUE nanosuspension (c) and placebo film (d).

Table 1
Mean size (*Z*-AVE) of QUE: bulk, freshly prepared nanosuspensions, freeze dried nanocrystals and nanocrystals after dissolution of both freshly prepared (day 0) and 6 month old film in water.

QUE	*Z*-AVE (nm)
Bulk	7400 ± 2300
Nanosuspension	753.5 ± 8.2
Freeze dried nanocrystals	920.7 ± 15.3
Film loaded nanocrystals (day 0)	781.5 ± 75.1
Film loaded nanocrystals (6 month)	795.6 ± 86.3

3.2. Morphological characterization

High pressure homogenization led to a QUE particle size reduction of about one order of magnitude. Indeed bulk QUE exhibited a mean particle size of 7.4 ± 2.3 μm while the freshly prepared QUE nanosuspension presented a *Z*-AVE of 753 nm (0.31 PI, (Fig. 4 and Tables 1 and 2).

The nanosuspension also exhibited a very highly negative zeta potential value (−51.7 mV), due to the presence of Tween 80, which should ensure high stability against re-aggregation phenomena. As shown in Table 2, during the first 30 days, QUE nanosuspensions maintained similar mean diameter and polydispersity index values. However, after three months of storage, the dimension and the polydispersity index slightly increased to 851 nm and 0.45, respectively, while the *Z* potential values were constant.

Freeze drying of the nanosuspensions permitted us to obtain nanocrystals with a particle size in agreement with the initial nanosuspension as showed by PCS analysis (Table 1) and the TEM images reported in Fig. 4. Nevertheless, after three months of storage the re-suspended nanocrystals exhibited two populations of

Table 2
Mean size (Z-AVE), polydispersity index (PI) and Z potential (ZP) of QUE nanosuspensions stored at 4 ± 1 °C and monitored during 90-day.

Day	(Z-AVE) (nm)	P.I.	ZP (mV)
0	753.5 ± 8.2	0.31 ± 0.05	−51.7 ± 1.3
1	752.9 ± 1.2	0.33 ± 0.03	−49.4 ± 0.8
7	761.3 ± 3.3	0.30 ± 0.07	−50.7 ± 0.1
14	757.3 ± 5.7	0.36 ± 0.06	−47.9 ± 1.0
30	783.6 ± 15	0.38 ± 0.02	−52.8 ± 1.3
60	843.7 ± 4.6	0.42 ± 0.02	−48.6 ± 0.9
90	851.1 ± 3.2	0.45 ± 0.02	−49.5 ± 1.6

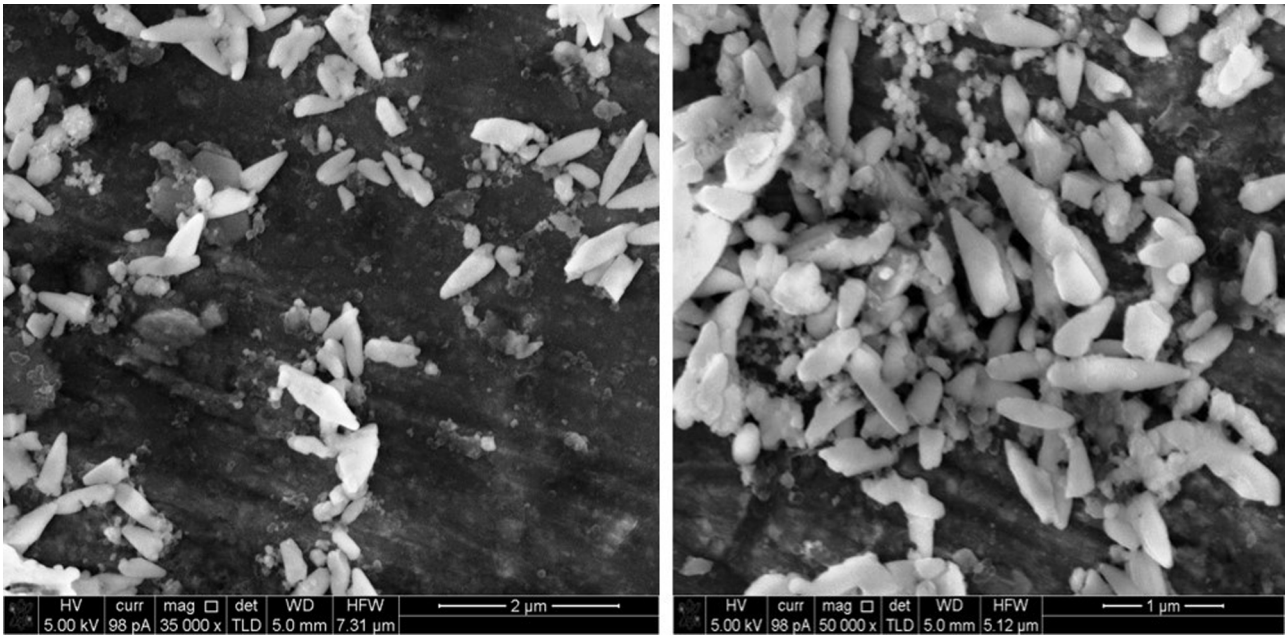

Fig. 4. QUE nanosuspension TEM images.

particles at about 700 nm (35.6% volume) and 7.8 μm (64.5% volume). This aggregation phenomenon could be due to the strong reduction of the *Z* potential value, which dropped to -17.9 ± 0.4 mV after three months of storage.

TEM images of MDX6 film loaded with QUE nanocrystals and the corresponding placebo film are shown in Fig. 5a and b. The former (Fig. 5a) disclosed a rough surface and showed, mixed with film matrix, several QUE nanocrystals arranged in different positions and orientations. This morphology completely differed from that of placebo films (Fig. 5b). In the placebo film, pores are evident but the crystals and surface roughness of the QUE nanocrystal-loaded film are absent.

Dissolution of the film in water led to the formation of a fine dispersion of the drug nanocrystals (795.6 ± 86.3 after 6 month of storage, Table 1) with no formation of aggregates or aggregates easily redispersible. The lack of aggregates can be attributed to both the high z-potential of the system -39.4 ± 1.1 mV and steric hindrance due to presence of MDX.

3.3. Technological characterization

Films were evaluated by determining their tensile properties, which are clearly related to the handling of the dosage form, and the QUE dissolution profile.

As far as the tensile properties are concerned, the loading of the QUE nanocrystals into the MDX6 film caused a variation of the film elasticity and ductility. Indeed, the elastic modulus (*Y*) of the loaded films was about half that of the placebo, while the elongation at break (*E* %) increased four fold (Table 3).

These data suggested that the QUE nanocrystals affect the mechanical properties, surprisingly acting as a non-conventional filler. Indeed, these results are in contrast with literature data

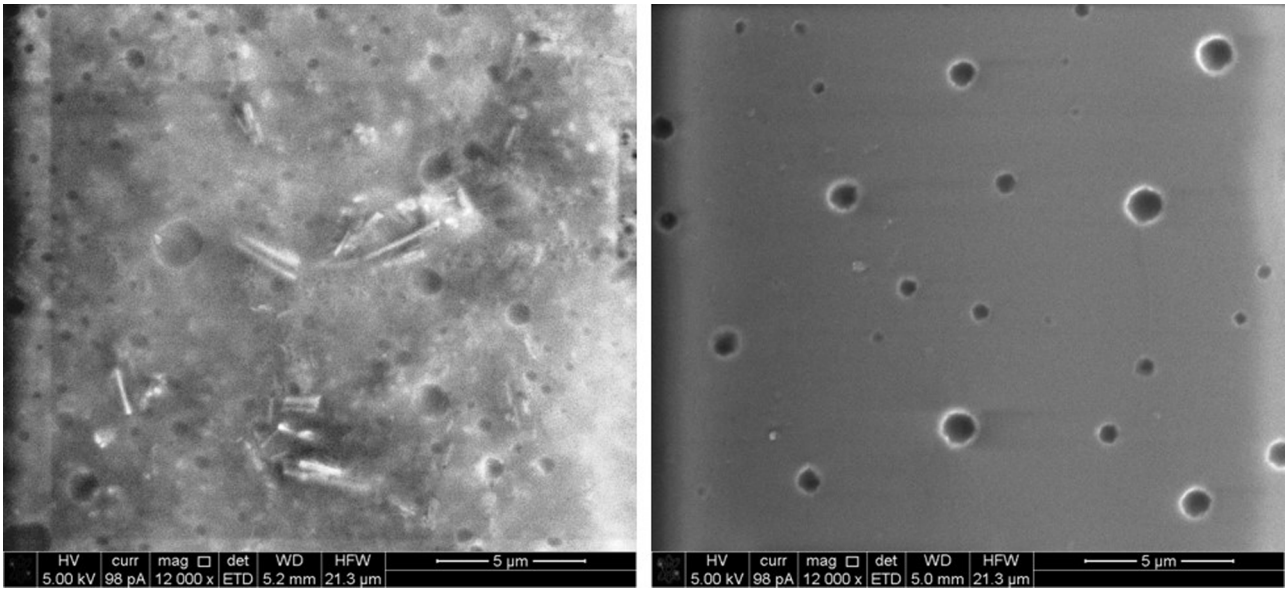

Fig. 5. (a) QUE nanosuspension loaded film TEM image; (b) placebo film TEM image.

Table 3
Thickness and tensile properties of the films.

	Thickness (μm)	*Y* (MPa)	TS (MPa)	*E* % (%)	*W* (MPa)
Placebo film	96.0	0.41 ± 0.17	0.88 ± 0.20	35 ± 6	0.21 ± 0.07
Drug loaded film	116.0	0.25 ± 0.04	0.53 ± 0.04	124 ± 39	0.56 ± 0.19

Y elastic modulus; TS tensile strength; *E* % elongation at break; *W* tensile energy to break.

concerning the addition to polysaccharide films of nanomaterials which are reported to be able to improve the mechanical properties of starch films by increasing their elasticity and tenacity (Alexandre & Dubois, 2000; Chen & Evans, 2005; Cyras, Manfredi, Ton-That, & Vázquez, 2008; Wilhelm, Sierakowski, Souza, & Wypych, 2003). However, our set of data is in agreement with those reported for polymethylmethacrylate–alumina films. In this last case, increasing the filler content, namely the alumina nanoparticles, the *Y* value dropped and the elongation at break increased about 8 fold. This anomalous behavior was justified considering that the alumina nanoparticles had very little interfacial interaction with the polymer matrix (Jordan, Jacob, Tannenbaum, Sharaf, & Jasiuk, 2005). The lack of interaction among QUE nanocrystals and MDX6 film is in agreement with the spectroscopic data and the lack of alteration of particle size and zeta potential of nanoparticles.

3.4. Dissolution studies

For drugs like QUE, characterized by poor water solubility, dissolution rate is the parameter which controls the rate of oral absorption. Therefore, in order to improve the dissolution rate, in this study we prepared QUE nanocrystals which we loaded into MDX6 fast dissolving films.

To study the dissolution behavior of bulk QUE, freeze dried QUE nanocrystals and QUE nanocrystal loading films, dissolution tests were performed in distilled water according to the United States Pharmacopeia using 10 mg of QUE in each sample. Samples withdrawn from the dissolution medium were analyzed by HPLC, to measure QUE content and stability. HPLC analyses showed no degradation products of the released QUE from all the tested formulations.

As reported in Fig. 6, bulk QUE showed the lowest dissolution rate, while faster dissolution profiles were clearly obtained by testing both free and film loaded nanocrystals. Indeed, size reduction from bulk QUE (7.4 ± 2.3 μm) to freeze dried QUE nanocrystals (920.7 ± 15.3 nm), significantly increased the dissolution rate which reached a maximum when nanosuspensions were loaded into the MDX6 films.

As predicted by the Noyes–Whitney dissolution model (Noyes & Whitney, 1897), the improvement in QUE dissolution rate was mainly determined by the increased surface-to-volume ratio due to the submicron size of the drug nanocrystals. However, also the decreasing of the diffusion layer thickness around nanocrystals, as described by the Prandtel equation (Möschwitzer & Müller, n.d.), as well as the increased saturation solubility, should result in an even faster dissolution rate (Kesisoglou, Panmai, & Wu, 2007). Furthermore, the partial amorphisation of QUE produced during nanocrystal preparation (high pressure homogenization process) could cause an increase in drug solution concentration and dissolution rate.

Meanwhile, the improvement in QUE dissolution rate obtained by films as compared to freeze dried nanocrystals, could be due to the lack of nanoparticle aggregates or more likely to the presence of easily dispersible aggregates in the MDX film. Because of the high solubility of MDX, a fine nanocrystal dispersion is rapidly obtained when the film is placed in water.

Indeed, nanoparticle agglomeration is almost inevitable after drying of nanosized products, and, therefore, the dissolution performance of loaded film QUE nanocrystals will not depend as much on the occurrence of agglomerates but rather on how easily they break up during dissolution (Wu, Zhang, & Watanabe, 2011).

As reported previously in the literature, agglomeration tendency and strength depend on the surface hydrophobicity of the particles, which therefore determines the extent to which preservation of the dissolution characteristics after drying is feasible. In the absence of a precise measurement, the log *P* value can be used to predict the hydrophobicity of nanoparticle surface. Indeed, log *P* higher than 4 usually indicates compounds for which the rate-limiting step in the dissolution process is the agglomerate disintegration (Van Eerdenbrugh et al., 2008). In our case, since QUE has a 1.82 log *P* value, the drying process during the MDX6 film leads to the formation of aggregates that are easily redispersible, as demonstrated

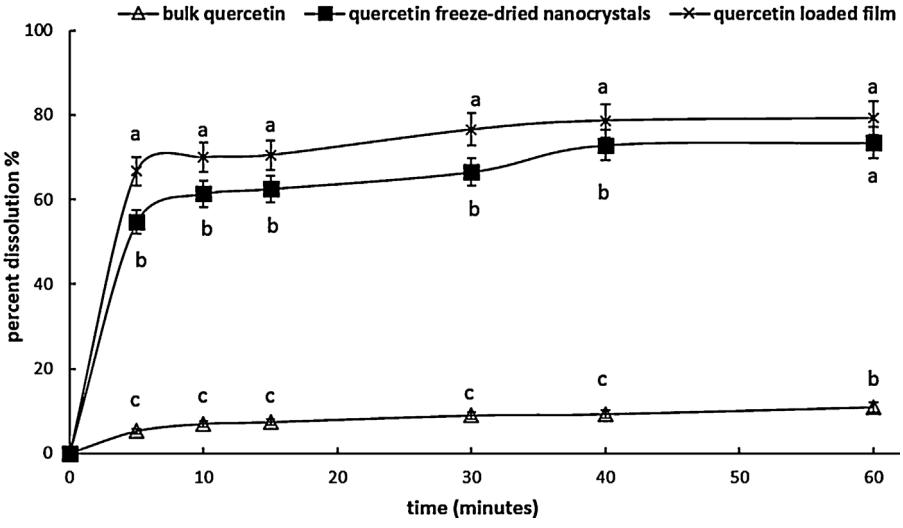

Fig. 6. Dissolution profiles for bulk QUE, QUE freeze-dried nanoscrystals and QUE loaded film. Different letters indicate significant differences at $P \leq 0.05$.

by both photon correlation spectroscopy measurements (Table 1) and dissolution profiles (Fig. 6). In particular, it can be noticed that after five minutes, the amounts of QUE dissolved from the fast dissolving films, freeze dried QUE nanocrystals and QUE raw material were 66.73%, 54.65% and 5.20% respectively.

4. Conclusions

The reduction of QUE size by means of high pressure homogenization with Tween 80 as stabilizer allowed us to obtain drug nanocrystal that could be easily incorporated in MDX6 films, avoiding stability issues associated with nanoparticles. It is interesting to note that the dissolution profile of QUE loaded in fast dissolving film was significantly faster than that from the free freeze-dried nanocrystals.

The overall picture which emerges is that fast dissolving films made of MDX6 can be advantageously used as solid dosage forms for oral delivery of QUE nanocrystals. Indeed, MDX films offer the opportunity of loading drug nanocrystals in a neutral and high soluble polysaccharide matrix, which provides long-term storage stability and fast dissolution rate.

Acknowledgement

Dr. Francesco Corrias was financed by Regione Autonoma della Sardegna under the Master and Back Programme, Reference code: PRR-MAB-A2011-18833. This work was partially supported by a grant from MIUR, Italy (PRIN 2010-2011, Prot. 2010H834LS_004). The authors are grateful to Dr. Antonella Sirigu of Agris (Cagliari) for her precious help with statistical calculations.

References

Alexandre, M., & Dubois, P. (2000). Polymer-layered silicate nanocomposites: Preparation, properties and uses of a new class of materials. *Materials Science and Engineering: R: Reports*, *28*(1–2), 1–63.

Cai, X., Fang, Z., Dou, J., Yu, A., & Zhai, G. (2013). Bioavailability of quercetin: Problems and promises. *Current Medicinal Chemistry*, *20*(20), 2572–2582.

Chen, B., & Evans, J. R. G. (2005). Thermoplastic starch–clay nanocomposites and their characteristics. *Carbohydrate Polymers*, *61*(4), 455–463.

Chessa, M., Caddeo, C., Valenti, D., Manconi, M., Sinico, C., & Fadda, A. M. (2011). Effect of penetration enhancer containing vesicles on the percutaneous delivery of quercetin through new born pig skin. *Pharmaceutics*, *3*(3), 497–509.

Cilurzo, F., Cupone, I. E., Minghetti, P., Buratti, S., Selmin, F., Gennari, C. G. M., et al. (2010). Nicotine fast dissolving films made of maltodextrins: A feasibility study. *AAPS PharmSciTech*, *11*(4), 1511–1517.

Cilurzo, F., Cupone, I. E., Minghetti, P., Selmin, F., & Montanari, L. (2008). Fast dissolving films made of maltodextrins. *European Journal of Pharmaceutics and Biopharmaceutics*, *70*(3), 895–900.

Cyras, V. P., Manfredi, L. B., Ton-That, M.-T., & Vázquez, A. (2008). Physical and mechanical properties of thermoplastic starch/montmorillonite nanocomposite films. *Carbohydrate Polymers*, *73*(1), 55–63.

De Mello Costa, A. R., Marquiafável, F. S., de Oliveira Lima Leite Vaz, M. M., Rocha, B. A., Pires Bueno, P. C., Amaral, P. L. M., et al. (2010). Quercetin-PVP K25 solid dispersions. *Journal of Thermal Analysis and Calorimetry*, *104*(1), 273–278.

Fatma, S., Talegaonkar, S., Iqbal, Z., Panda, A. K., Negi, L. M., Goswami, D. G., et al. (2014). Novel flavonoid-based biodegradable nanoparticles for effective oral delivery of etoposide by *P*-glycoprotein modulation: An in vitro, ex vivo and in vivo investigations. *Drug Delivery*, 1–12.

Garnero, C., Chattah, A. K., & Longhi, M. (2013). Supramolecular complexes of maltodextrin and furosemide polymorphs: A new approach for delivery systems. *Carbohydrate Polymers*, *94*(1), 292–300.

Harwood, M., Danielewska-Nikiel, B., Borzelleca, J. F., Flamm, G. W., Williams, G. M., & Lines, T. C. (2007). A critical review of the data related to the safety of quercetin and lack of evidence of in vivo toxicity, including lack of genotoxic/carcinogenic properties. *Food and Chemical Toxicology*, *45*(11), 2179–2205.

Jordan, J., Jacob, K. I., Tannenbaum, R., Sharaf, M. A., & Jasiuk, I. (2005). Experimental trends in polymer nanocomposites—A review. *Materials Science and Engineering, A*, *393*(1-2), 1–11.

Kelly, G. S. (2011). Quercetin. Monograph. *Alternative Medicine Review: A Journal of Clinical Therapeutic*, *16*(2), 172–194.

Kesisoglou, F., Panmai, S., & Wu, Y. (2007). Nanosizing—Oral formulation development and biopharmaceutical evaluation. *Advanced Drug Delivery Reviews*, *59*(7), 631–644.

Kocbek, P., Baumgartner, S., & Kristl, J. (2006). Preparation and evaluation of nanosuspensions for enhancing the dissolution of poorly soluble drugs. *International Journal of Pharmaceutics*, *312*(1–2), 179–186.

Lai, F., Pini, E., Corrias, F., Perricci, J., Manconi, M., Fadda, A. M., et al. (2014). Formulation strategy and evaluation of nanocrystal piroxicam orally disintegrating tablets manufacturing by freeze–drying. *International Journal of Pharmaceutics*, *467*(1–2), 27–33.

Lai, F., Pini, E., Angioni, G., Manca, M. L., Perricci, J., Sinico, C., et al. (2011). Nanocrystals as tool to improve piroxicam dissolution rate in novel orally disintegrating tablets. *European Journal of Pharmaceutics and Biopharmaceutics*, *79*(3), 552–558.

Leathers, T. D. (2003). Biotechnological production and applications of pullulan. *Applied Microbiology and Biotechnology*, *62*(5-6), 468–473.

Li, B., Konecke, S., Harich, K., Wegiel, L., Taylor, L. S., & Edgar, K. J. (2013). Solid dispersion of quercetin in cellulose derivative matrices influences both solubility and stability. *Carbohydrate Polymers*, *92*(2), 2033–2040.

Li, B., Zhang, L., Deng, Y., & Liang, N. (2004). Study on solid dispersion of quercetin–PEG(6000). *Huaxi Yaoxue Zazhi*, *19*, 35–37.

Möschwitzer, J., Müller, R. H. (n.d.). Drug Nanocrystals—The Universal Formulation Approach for Poorly Soluble Drugs, Nanoparticulate Drug Delivery Systems, Informa Healthcare.(first edit.).

Müller, R. H., Gohla, S., & Keck, C. M. (2011). State of the art of nanocrystals—Special features, production, nanotoxicology aspects and intracellular delivery. *European Journal of Pharmaceutics and Biopharmaceutics*, *78*(1), 1–9.

Nijveldt, R. J., van Nood, E., van Hoorn, D. E., Boelens, P. G., van Norren, K., & van Leeuwen, P. A. (2001). Flavonoids: A review of probable mechanisms of action and potential applications. *American Journal of Clinical Nutrition*, *74*(4), 418–425.

Noyes, A. A., & Whitney, W. R. (1897). The rate of solution of solid substances in their own solutions. *Journal of the American Chemical Society*, *19*(12), 930–934.

Okamoto, T. (2005). Safety of quercetin for clinical application. *International Journal of Molecular Medicine*, *16*(2), 275–278 (Review).

Pinna, M., Pinna, F. (2009, November). Quick water-dissolving film containing cosmetic, aromatic, pharmaceutical or food substances. US7612048.

Ribeiro, M. E. N. P., Vieira, I. G. P., Cavalcante, I. M., Ricardo, N. M. P. S., Attwood, D., Yeates, S. G., et al. (2009). Solubilisation of griseofulvin, quercetin and rutin in micellar formulations of triblock copolymers E62P39E62 and E137S18E137. *International Journal of Pharmaceutics*, *378*(1–2), 211–214.

Sahoo, N. G., Kakran, M., Shaal, L. A., Li, L., Müller, R. H., Pal, M., et al. (2011). Preparation and characterization of quercetin nanocrystals. *Journal of Pharmaceutical Sciences*, *100*(6), 2379–2390.

Selmin, F., Franceschini, I., Cupone, I. E., Minghetti, P., & Cilurzo, F. (2015). Aminoacids as non-traditional plasticizers of maltodextrins fast-dissolving films. *Carbohydrate Polymers*, *115*, 613–616.

Shen, B., Shen, C., Yuan, X., Bai, J., Lv, Q., Xu, H., et al. (2013). Development and characterization of an orodispersible film containing drug nanoparticles. *European Journal of Pharmaceutics and Biopharmaceutics*, *85*(3 Pt. B), 1348–1356.

Utesch, D., Feige, K., Dasenbrock, J., Broschard, T. H., Harwood, M., Danielewska-Nikiel, B., et al. (2008). Evaluation of the potential in vivo genotoxicity of quercetin. *Mutation Research*, *654*(1), 38–44.

Van Eerdenbrugh, B., Froyen, L., Van Humbeeck, J., Martens, J. A., Augustijns, P., & Van den Mooter, G. (2008). Drying of crystalline drug nanosuspensions-the importance of surface hydrophobicity on dissolution behavior upon redispersion. *European Journal of Pharmaceutical Sciences*, *35*(1-2), 127–135.

Wilhelm, H.-M., Sierakowski, M.-R., Souza, G. P., & Wypych, F. (2003). Starch films reinforced with mineral clay. *Carbohydrate Polymers*, *52*(2), 101–110.

Wu, L., Zhang, J., & Watanabe, W. (2011). Physical and chemical stability of drug nanoparticles. *Advanced Drug Delivery Reviews*, *63*(6), 456–469.

Zerbe, H. G., Guo, J. H. (1998, May). Zubereitung zur Anwendung in der Mundhöhle mit einer an der Schleimhaut haftklebenden, Pharmazeutika oder Kosmetika zur dosierten Abgabe enthaltenden Schicht. DE19646392.

Zheng, Y., & Chow, A. H. L. (2009). Production and characterization of a spray-dried hydroxypropyl-beta-cyclodextrin/quercetin complex. *Drug Development and Industrial Pharmacy*, *35*(6), 727–734.